

EUROPEAN COOPERATION  
IN SCIENCE  
AND TECHNOLOGY

CA20120 TD(22)01063

Bologna, Italy

February 8-11, 2022

---

EURO-COST

---

SOURCE: UCL, Universite catholique de Louvain, Belgium  
ULB, Universite libre de Bruxelles, Belgium

**Joint rate and power density analysis in Manhattan environments: (a comparison of) stochastic geometry and ray-tracing approaches**

**Simon Demey, Charles Wiame, Claude Oestges and Philippe De Doncker**

Place du levant 3, 1348 Louvain-la-Neuve

Phone: +32 10 47 23 10

Fax:

Email: [simon.demey@uclouvain.be](mailto:simon.demey@uclouvain.be)

# Joint rate and power density analysis in Manhattan environments: (a comparison of) stochastic geometry and ray-tracing approaches

Simon Demey, *Member, IEEE*, Charles Wiame, *Member, IEEE*,  
Claude Oestges, *Fellow, IEEE*, and Philippe De Doncker, *Fellow, IEEE*

## Abstract

The proposed work tries to quantify how relevant it is to use a deterministic channel model like ray tracing at a network deployment level in a Manhattan-like environment. More precisely, the goal is to compare it with simpler and more computationally efficient models to see if similar results can be obtained at a lower cost. In the framework of the analysis, ray tracing is thus compared to a stochastic geometry-based model in terms of coverage probability and exposure at a centric user for which we were able to derive semi-closed form expressions. In addition, a good lower bound for the joint coverage-exposure distribution was found. In order to easily mimic the propagation mechanisms implemented in the UCLouvain RT software and enable fair comparison, the Berg recursive model was considered as channel model. Finally, the analytical expressions were further enhanced to take into account the antenna height as well as the line-of-sight probability in the typical street and to distinguish a typical user located at a crossroad from a typical user located inside a street.

## Index Terms

EMF exposure, stochastic geometry, ray tracing.

## I. INTRODUCTION

From Bell Labs perspective, the global data traffic is expected to skyrocket in future wireless networks [1]. This is due to the ever-growing number of mobile devices and the growing usage of applications which happen to be more and more data hungry [2]. For those reasons, 1000 times the 4G capacity has been set as objective for future 5G networks [3].

In order to withstand this significant increase in capacity demand, heterogeneous networks (Hetnets) will become the norm. In fact, small cells will be used to complement already existing macrocells where most needed in order to offload macrocells to achieve better spectral efficiency and to extend their coverage region. It is expected to find up to 40-50 BSs/km<sup>2</sup> [4].

With the arrival of 5G communications systems, a wide variety of links will then have to coexist in the same area [3]. In addition, new 5G features are currently under research to boost the total capacity which broadens even more the link types panel. Among them, we have:

- Massive Machine-Type Communication (mMTC): communications between sensors for surveillance, communications between devices in a smart home, etc...
- Ultra-dense networks (UDN) with targeted user data rates around 10Gbps. UDNs are said to require large bandwidth hence the investigation of millimeter-wave (mmW) bands that raises further challenges.
- Moving BSs (on public transport, on drones, etc...).
- Device-to-device (D2D) communications.
- Very large antenna arrays.

For this reason, new channel models are expected to handle all those new aspects. On the one hand, network densification and multi-service operations will push towards site- and service-specific simulations which could make deterministic models like ray tracing (RT) more suitable.

On the other hand, given the large randomness in future networks as well as the variable user density and network topology, it is not clear if stochastic models cannot fulfil the same goal at a cheapest simulation cost while deploying the network at a larger scale. In this case, we generally abstract some of the link-level details due to limited time and computational resources as we want to easily get insight about the network performances. In fact, in order to deploy new technologies, their impact on the network performances has to be quantified and validated [2]. To do so, a link analysis is not sufficient due to the always present randomness and a larger scale analysis is essential which makes stochastic geometry (SG) a suitable mathematical tool. Moreover, many 5G technologies have already been investigated using SG as shown in [5].

#### *A. Brief overview of related works*

Regarding urban environment stochastic models, [6] first introduced the use of the Manhattan Poisson Line Process (MPLP) to model roads inside SG models. The coverage probability for a typical UE using a simple distance-based LOS path loss model and a blockage (shadowing)-based NLOS path loss model. [7] derives closed-form expression for the same metric for vehicular networks operating at mmWave frequencies.

Other works also considered the use of a generalization of the MPLP, namely the Cox process, in the analysis of wireless networks [8, 9].

[10] provides a complete tutorial on how to compute several metrics of interest for BS distributed following a beta-Ginibre point process, a Matèrn hard core point process as well as a Poisson point process. Some of the metrics studied in the framework of this document are directly taken from this tutorial and adapted to a case where BSs are located in the streets distributed by means of a MPLP.

While many works focussed on the analysis of emerging networks using SG theory, almost nothing can be found about the models validation using other techniques.

In [11], experimental validation of stochastic models has been done for the coverage probability of the O2 and Vodafone deployments in the cities of London and Manchester.

More recently, [12] validated stochastic models for what they call the radar detection coverage probability using finite difference time domain technique.

To the best of the author knowledge, no validation of SG models using RT can be found in the litterature. This is certainly due to the fact that it is a time-consuming procedure which however do not affect its relevance.

### *B. Contributions*

On the basis of the aforementioned works, the main findings of this study can be summarized as follows:

- We fully revisit the Manhattan model orginally presented in [6]. A number of features are added to this model to capture more propagation aspects, and make the results closer to the reality. These new characteristics include: :
  - The use of a diffraction model to take into account power contributions coming from bases stations located in avenues perpendicular to the user street. To this purpose, Berg recursive model is thus selected for its simplicity and its fair accuracy regarding the path loss level [13]. As explained in [14], the contributions from diffraction can be significant compared to building penetration hence the need to address their modelling.
  - Unlike [6], where the small scale fading was only Rayleigh, our framework enable to incorporate any fading distribution in the model. We decided to incorporate Rician fading but the model could be easily generalized to other fading models.

- We include the presence of street obstacles (cars, trucks,...) by means of a blockage model represented by means of distance dependent line-of-sight and non-line of sight probabilities.
- In practical deployments, a non-negligible proportion of users can be located at street intersections. Due the simultaneous presence of LoS BSs located in the two perpendicular streets, the power levels measured at the user can significantly differ from the users that are not located at a crossroad. In the original work of [6], the users are almost surely never located at a street intersection. Our work include a non-zero probability for the typical user to be located at a street intersection, and takes into account the presence of power signals coming from two streets.
- The height difference between the UE and the BSs is here taken into account as it might considerably affect the different metrics of interest. In fact, neglecting this difference leads to an overestimation of the contributions coming from BSs located in the close vicinity.
- To the best of the authors knowledge, this treatise is the first work studying EMF exposure in a Poisson line process. In order to fully characterize the statistics of this exposure, and its correlation to the spectral efficiency, the following performance metrics are calculated:
  - Marginal disitributions of the exposure and rate
  - Joint rate and exposure distribution
- The proposed work gives a first comparison between stochastic geometry and RT on several metrics of interest for a Manhattan-like environment. While many works have studied the impact of key network parameters on the network performances by means of SG, almost nothing can be found about the validation of the observations made with this approach using deterministic models. For this reason, the proposed study tries to fill this gap by running RT simulations as if they were Monte Carlo Simulations in order highlight the similarities and differences for the different metrics for which semi-closed form expressions were derived

using the Gil-Pelaez theorem [15].

### C. Organization of the paper

The system model used in this work as well as the studied metrics are introduced and defined in Section II. Analytical expressions for those metrics are derived using SG in Section III. Numerical results are grouped in Section IV. Section V finally summarizes the key takeaways and provides some future research directions.

*Notations:*  $h_{ij}$  will always refer to the normalized power fading coefficient on the link between transceiver  $i$  and transceiver  $j$ . In this work, all coefficients are supposed to be independently distributed even if some correlation might exist on the power fading coefficients of similar links.  $d_{ij}$  will always refer to the euclidian distance between transceiver  $i$  and transceiver  $j$ .

## II. SYSTEM MODEL

### A. Network topology

We consider the downlink part of a cellular network deployed in  $\mathbb{R}^2$  on a square region  $L \times L$  and operated at a frequency  $f$ . Avenues (vertical) and streets (horizontal) are drawn using two independent Manhattan Poisson line processes (MPLP)  $\Phi_{av}$  and  $\Phi_{st}$  with the same intensity  $\lambda_S$ . Base stations (BSs) are deployed in each street or avenue using a independent one-dimensional Poisson point process (PPP) of intensity  $\lambda_B$ . All BSs are assumed to be equipped with a single isotropic antenna with unit antenna gain emitting with the same power  $P_B$ . Finally, all BS are supposed to be placed at a height  $h_B$ .

We perform a network analysis for a single typical UE  $i^*$ , located at  $(0, 0, h_U)$ . This UE is assumed to be located in the so-called typical street. This typical street is by definition a street of ordinate  $y = 0$  or an avenue of ordinate  $x = 0$ . The typical UE is said to receive power with

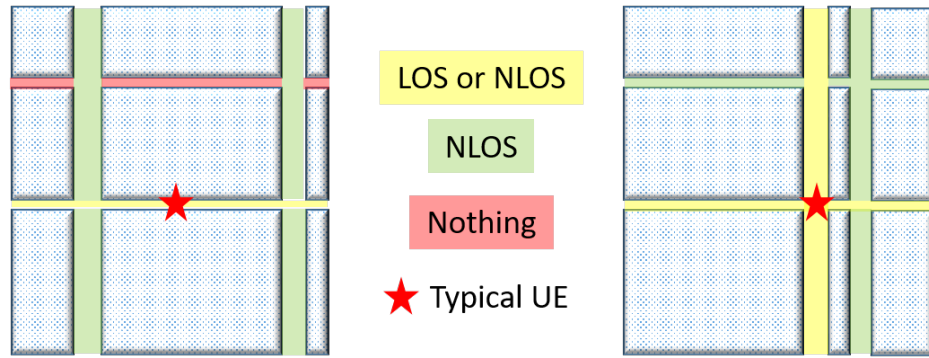


Fig. 1: Left: Street UE. Right: Crossroad UE. The street UE receives LOS/NLOS contributions from its typical street and NLOS diffracted contributions from the perpendicular avenues but receives nothing from parallel streets. On the contrary, the crossroad UE receives LOS/NLOS contributions from its typical street and avenue and NLOS diffracted contributions from the perpendicular avenues and streets.

a single isotropic antenna with unit antenna gain.

As previously mentioned, if the typical UE is placed at a crossroad, he will certainly experience different performances. For this reason, the general user can be defined to be present:

- at a crossroad, with probability<sup>1</sup>  $\eta$
- in a street, with probability  $1 - \eta$ .

For sake of simplicity, we will respectively refer to a typical UE located in a street and at a crossroad as a street UE and a crossroad UE. In this document, expressions with the subscript '1' will refer to the street UE and expressions with the subscript '2' will refer to the crossroad UE. The difference between both types of UEs is highlighted in Figure 1.

In the framework of the RT simulations, almost everything stays unchanged but

<sup>1</sup>This probability  $\eta$  can for instance be defined as the ratio between the streets and building widths

- Streets and avenues are given a non-zero width  $w_S$ .
- Buildings all have the same height  $h_{BU}$ .
- The side of the road for each BS is randomly chosen. Those are placed at a distance  $d_{B,BU}$  from the buildings walls.

## B. Power computation

1) *Ray Tracing*: In recent years, ray tracing has been extensively used to model the channel between a given base station (BS) and a given user (UE) in a deterministic way given the surrounding environment. For this reason, we decided to develop our own tool here at UCLouvain and validated it. While many propagation mechanisms exist, only two types are taken into account by this tool: reflection and diffraction (i.e. scattering and other more complex mechanisms are here disregarded). In addition, only outdoor to outdoor scenarios are considered which means both the UE and the BS are exclusively located outside the buildings and so are the paths we identify between those two transmitters. The conventions used for reflection and diffraction are depicted on Figure 2 and 3.

To keep the computational time in a reasonable range, at most two interactions are considered between a transmitting BS and a receiving UE. In addition, diffraction is only acknowledged on the last interaction. Those hypotheses seems not to be too restrictive as an electromagnetic wave which undergone more than two interactions or more than one diffraction is strongly attenuated.

Down below, you will find how the electrical fields  $\in \mathbb{R}^3$  are computed when undergoing the different propagation mechanisms.

### **Line of sight**

Supposing  $\overline{E}_0$  is the transmitted electric field, the LOS field at an observation point P is given

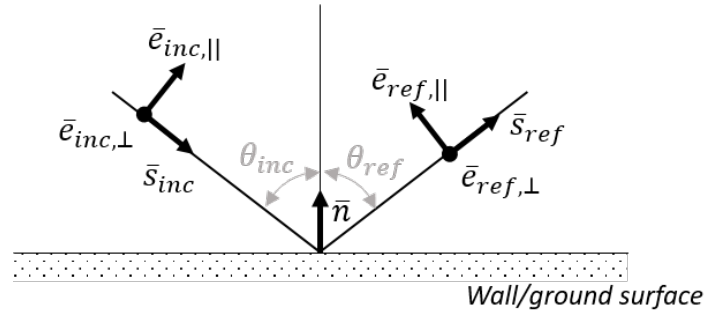


Fig. 2: Conventions: reflection (reproduced from [16])

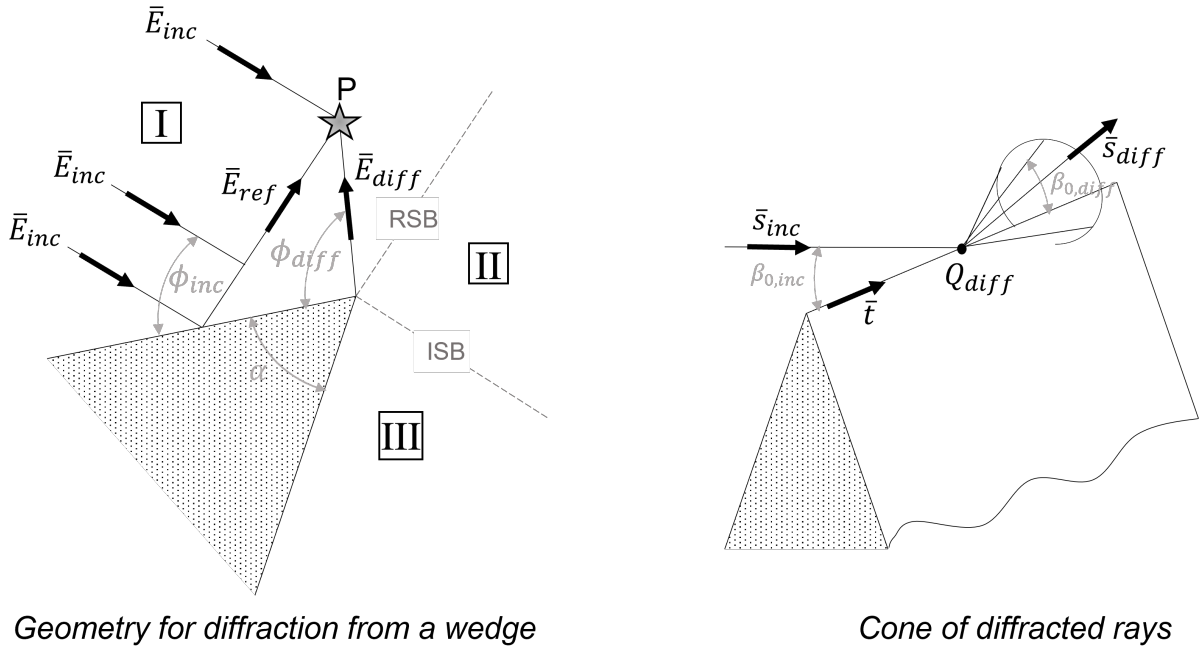


Fig. 3: Conventions: diffraction (reproduced from [16])

by:

$$\bar{E}_{LOS}(P) = \bar{E}_0 \frac{e^{-jkd_{BSP}}}{d_{BSP}} \quad (1)$$

where  $k$  is the wave number and  $d_{BSP}$  is the distance between the transmitting BS and the observation point.

### Reflection

Supposing  $\bar{E}_{inc}(Q_{ref})$  is the incoming field at the reflection point  $Q_{ref}$ , the reflected field  $\bar{E}_{ref}(P)$  at observation point P is given by :

$$\bar{E}_{ref}(P) = \bar{\bar{R}} \cdot \bar{E}_{inc}(Q_{ref}) \frac{d_{IQ}}{d_{IQ} + d_{QR}} e^{-jkd_{QR}} \quad (2)$$

where  $d_{IQ}$  is the distance between the field source and the reflection point,  $d_{QR}$  is the distance between the reflection point and the observation point and  $\bar{\bar{R}}$  is the Fresnel dyadic coefficient.  $\bar{\bar{R}}$  can be computed as follows:

$$\bar{\bar{R}} = R_{\parallel} \bar{e}_{inc,\parallel} \bar{e}_{ref,\parallel} + R_{\perp} \bar{e}_{inc,\perp} \bar{e}_{ref,\perp} \quad (3)$$

$$R_{\parallel} = \frac{\epsilon_{r,eff} \cos(\theta_{inc}) - \sqrt{\epsilon_{r,eff} - \sin^2(\theta_{inc})}}{\epsilon_{r,eff} \cos(\theta_{inc}) + \sqrt{\epsilon_{r,eff} - \sin^2(\theta_{inc})}} \quad (4) \quad R_{\perp} = \frac{\cos(\theta_{inc}) - \sqrt{\epsilon_{r,eff} - \sin^2(\theta_{inc})}}{\cos(\theta_{inc}) + \sqrt{\epsilon_{r,eff} - \sin^2(\theta_{inc})}} \quad (5)$$

where  $\theta_{inc}$  is the incidence angle with respect to the plane normal and  $\epsilon_{r,eff}$  is the relative electrical permittivity.

### Diffraction

Using uniform theory (UTD) of diffraction and supposing  $\bar{E}_{inc}(Q_{diff})$  is the incoming field at the reflection point  $Q_{diff}$ , the reflected field  $\bar{E}_{diff}(P)$  at observation point P is given by :

$$\bar{E}_{diff}(P) = \bar{\bar{D}} \cdot \bar{E}_{inc}(Q_{diff}) \sqrt{\frac{d_{IQ}}{d_{QR}(d_{IQ} + d_{QR})}} e^{-jkd_{QR}} \quad (6)$$

where  $d_{IQ}$  is the distance between the field source and the reflection point,  $d_{QR}$  is the distance between the reflection point and the observation point and  $\bar{\bar{D}}$  is the UTD dyadic coefficient.  $\bar{\bar{D}}$  can be computed as follows:

$$\bar{\bar{D}} = -D_s \bar{\beta}_{0,inc} \bar{\beta}_{0,diff} - D_h \bar{\phi}_{inc} \bar{\phi}_{diff} \quad (7)$$

$$\bar{\phi}_{inc} = \frac{\bar{s}_{inc} \times \bar{t}}{|\bar{s}_{inc} \times \bar{t}|} \quad (8)$$

$$\bar{\beta}_{0,inc} = \bar{\phi}_{inc} \times \bar{s}_{inc} \quad (9)$$

$$\bar{\phi}_{diff} = \frac{\bar{t} \times \bar{s}_{diff}}{|\bar{t} \times \bar{s}_{diff}|} \quad (10)$$

$$\bar{\beta}_{0,diff} = \bar{\phi}_{diff} \times \bar{s}_{diff} \quad (11)$$

where  $\bar{t}$  is a unitary vector tangential to the edge,  $\bar{s}_{inc}$  is the unitary incident direction vector,  $\bar{s}_{diff}$  is the unitary diffracted direction vector. Initially, the coefficients  $D_s$  and  $D_h$  should be computed as in [16]. However, to ensure reciprocity by changing the face assignment (“o-” or “n-faces”) depending on the region from which the incident ray is coming, we use Guevara’s coefficients instead. The angles used to compute Fresnel reflection coefficients are then also slightly adapted as explained in [17]. Their mathematical expressions are omitted in this document

### Received power

Finally, assuming  $\bar{E}_0$  is normalized at the emission, the received power at a typical user location  $i^*$  from a given BS  $j$  is given by

$$\bar{E}_{tot} = \sum_{n=1}^{N_{paths}} \bar{E}_{n,j} \quad (12)$$

$$P_{[W]}^{i^*j} = P_B \kappa^{-1} \|\bar{E}_{tot} \cdot \bar{E}_{tot}^H\| \quad (13)$$

where  $N_{paths}$  is the number of paths coming from this BS and arriving at the typical user under the considered hypotheses.  $\bar{E}_{n,j}$  are the corresponding electric fields at the typical user computed by means of Equations (1), (2) and (6).  $\kappa = (4\pi f/c)^2$  is the frequency-dependant attenuation ( $c$  being the speed of light).

2) *Stochastic Geometry*: Throughout this analysis, three different types of received signals will be taken into account in order to mimic what is computed with the ray tracing tool. For BSs located in the typical street, the BS has a distance-dependant probability  $p_L(r)$  to be in LOS with the typical UE and a distance-dependant probability  $p_N(r) = 1 - p_L(r)$  to have no

LOS with the typical UE. Supposing a typical UE  $i^*$  in the studied network:

### **Line of sight BS in the typical street**

The line-of-sight (LOS) signals are supposed to account for direct and reflected waves originating from the considered BS. The power received from a certain BS  $j$  is given by:

$$P_{[W]}^{i^*j} = P_B \kappa^{-1} \left| h_{i^*j}^{t,L} \right|^2 d_{i^*j}^{-\alpha_L^t} \quad (14)$$

where  $\alpha_L^t$  is the path loss coefficient on LOS signals originating from BSs in the typical street.

### **Non line of sight BS in the typical street**

The non line-of-sight (NLOS) signals are supposed to account for reflected waves originating from the considered BS. The power received from a certain BS  $j$  is given by:

$$P_{[W]}^{i^*j} = P_B \kappa^{-1} \left| h_{i^*j}^{t,N} \right|^2 d_{i^*j}^{-\alpha_N^t} \quad (15)$$

where  $\alpha_N^t$  is the path loss coefficient on NLOS signals originating from BSs in the typical street.

### **BS located in perpendicular streets or avenues**

Those signals are supposed to account for diffraction by buildings edges coming from BSs located in streets or avenues that are perpendicular to the typical street (and avenue for a crossroad UE).

Following Berg recursive method [13], the power received from a certain BS  $j$  is given by:

$$P_{RT,[W]}^{i^*j} = P_B \kappa^{-1} \left| h_{i^*j}^{p,N} \right|^2 d_n^{-\alpha_N^p} \quad (16)$$

where  $\alpha_N^p$  is the path loss coefficient on NLOS signals and  $d_n$  ( $n$  represents the number of diffractions) is the Berg distance which is actually higher than the real distance between UE  $i^*$

and BS  $j$ . This distance can be computed by means of the following recursion:

$$\begin{cases} d_n = k_n s_{n-1} + d_{n-1} \\ d_0 = 0, k_0 = 1 \end{cases} \quad (17)$$

with  $k_n = k_{n-1} + d_{n-1} q_{n-1}$  and  $q_n = q_{90} \left(\frac{\theta_n}{90}\right)^\nu$ . The consecutive distances  $s_n$  and angles  $\theta_n$  are computed using the conventions of Figure 4 where each dot represents a new diffraction on a new edge.

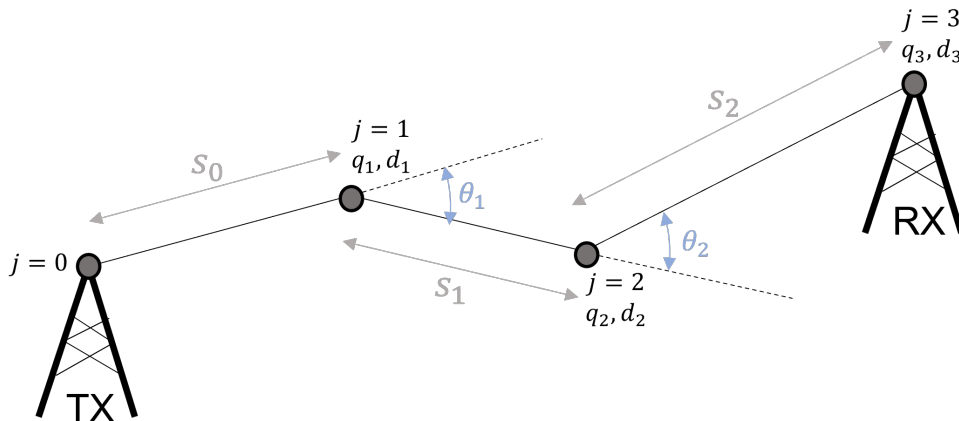


Fig. 4: Berg recursive model

The Berg recursive method is semi-empirical and its two parameters  $q_{90}$  and  $\nu$  are fixed by fitting the model to measurements data as it was done in the METIS project [18].  $q_{90}$  accounts for the diffraction loss caused by each node and a larger value means a larger loss. This parameter is given by:

$$q_{90} = \sqrt{\frac{q_\lambda}{\lambda}} \quad (18)$$

where  $q_\lambda$  is a frequency dependent model parameter and  $\lambda$  is the wavelength. If the system is operated at a frequency between 2 and 6 GHz,  $q_\lambda$  can be fixed at 0.031 for urban micro-cells [18].  $\nu$  accounts for how fast the loss changes in the transition zone between LOS and NLOS.

This second parameter is not useful in this model as all angles  $\theta_n$  are  $90^\circ$ .

In the framework of this study, distance-dependant Rician fading with K-factor  $K(r)$  will be assumed for contributions originating from the typical street and avenue while Rayleigh fading will be considered for diffracted contributions.

### C. Association policy

The typical UE associates to the closest base station of its typical street/avenue. Also, the path loss model in  $r^{-\alpha}$  has the advantage of being simple in a SG framework but it has a singularity at  $r = 0$  and provides unrealistic values for  $r < r_0 = 1$ . To solve this issue, it is assumed that no street intersection and no BS are generated in the segment  $[-r_0; r_0]$  around the typical user. If the antenna height difference (defined as  $h_B - h_U$ ) is higher than 1, this last condition can be disregarded for BSs.

Assuming closest BS association policy, the distribution function of the distance to the serving station for a street UE is given by [19]. This distribution is then slightly modified to take the prohibited zone  $[-r_0; r_0]$  into account as follows:

$$f_{r,1}(r) = \frac{2\lambda_B e^{-2\lambda_B r}}{e^{-2\lambda_B r_0} - e^{-2\lambda_B L}}, \quad \text{for } r_0 < r < L. \quad (19)$$

As the crossroad typical UE can connect to either the closest BS in its typical street or to the closest BS in its typical avenue, this distribution can be modified as:

$$f_{r,2}(r) = \frac{4\lambda_B e^{-4\lambda_B r}}{e^{-4\lambda_B r_0} - e^{-4\lambda_B L}}, \quad \text{for } r_0 < r < L \quad (20)$$

and its associated BS is on average two times closer.

### D. Global metrics

In the following definitions,  $N_B$  will refer to the number of BSs present in a given simulation.

1) *Coverage probability*: The coverage probability is defined as

$$P_c(\theta) = \mathbb{P} \left[ \text{SIR}_{i^*} > \theta \right] \quad (21)$$

where

$$\text{SIR}_{i^*} = \frac{P_{[W]}^{i^*j^*}}{\sum_{\substack{j \in [1, \dots, N_B] \\ j \neq j^*}} P_{[W]}^{i^*j}}. \quad (22)$$

and  $j^*$  is the index of the associated BS.

2) *CDF of the exposure*: This CDF of the exposure is defined as

$$P_e(\theta') = \mathbb{P} \left[ \text{Exp}_{i^*} < \theta' \right]. \quad (23)$$

where

$$\text{Exp}_{i^*} = \sum_{j \in [1, \dots, N_B]} P_{[W]}^{i^*j} \quad (24)$$

3) *Lower bound on the joint SIR-exposure distribution*: It might be interesting for an operator to jointly analyze the network coverage, as well as the exposure affecting the mobile user. For this reason, we define the double-threshold function

$$F(\theta, \theta') = \mathbb{P} \left[ \text{SIR}_{i^*} > \theta, \text{Exp}_{i^*} < \theta' \right]. \quad (25)$$

In the following section, we provide the expression of a function  $\bar{F}(\theta, \theta')$ , which is a lower bound on  $F(\theta, \theta')$ .

4) *CCDF of the capacity*: The CCDF of the capacity is defined as

$$P_{cap}(\theta'') = \mathbb{P} \left[ B \log_2 (1 + \text{SIR}_{i^*}) > \theta'' \right] \quad (26)$$

where  $B$  is the bandwidth.

### III. ANALYTICAL RESULTS

#### A. Preliminaries

We start by introducing a few characteristic functions, which will be useful to compute the different metrics for the different types of UEs. In the following expressions, we will assume  $dH = h_B - h_U$  to be the height difference between BSs and the typical UE.

1) *User located in a street:* Conditioned on  $r$ , the distance between the typical UE and its serving BS, the characteristic function of the useful received power is given by

$$\phi_{S,1}(t, \alpha|r) = \frac{K(r) + 1}{K(r) + 1 - jtP_B\kappa^{-1}\sqrt{r^2 + dH^2}^{-\alpha}} \exp \left[ \frac{K(r)jtP_B\kappa^{-1}\sqrt{r^2 + dH^2}^{-\alpha}}{K(r) + 1 - jtP_B\kappa^{-1}\sqrt{r^2 + dH^2}^{-\alpha}} \right] \quad (27)$$

where  $\alpha = \alpha_L^t$  if the serving BS is in LOS and  $\alpha = \alpha_N^t$  if the serving BS is not in LOS.

Conditioned on  $r$ , the characteristic function of the LoS interference coming from the typical street is given by

$$\phi_{L,1}(t|r) = \exp \left[ 2\lambda_B \int_r^L p_L(r') \left[ \frac{K(r') + 1}{K(r') + 1 - jtP_B\kappa^{-1}\sqrt{r'^2 + dH^2}^{-\alpha_L^t}} \exp \left( \frac{K(r')jtP_B\kappa^{-1}\sqrt{r'^2 + dH^2}^{-\alpha_L^t}}{K(r') + 1 - jtP_B\kappa^{-1}\sqrt{r'^2 + dH^2}^{-\alpha_L^t}} \right) - 1 \right] dr' \right]. \quad (28)$$

Conditioned on  $r$ , the characteristic function of the NLoS interference coming from the typical street is given by

$$\phi_{N,1}(t|r) = \exp \left[ 2\lambda_B \int_r^L p_N(r') \left[ \frac{K(r') + 1}{K(r') + 1 - jtP_B\kappa^{-1}\sqrt{r'^2 + dH^2}^{-\alpha_N^t}} \exp \left( \frac{K(r')jtP_B\kappa^{-1}\sqrt{r'^2 + dH^2}^{-\alpha_N^t}}{K(r') + 1 - jtP_B\kappa^{-1}\sqrt{r'^2 + dH^2}^{-\alpha_N^t}} \right) - 1 \right] dr' \right]. \quad (29)$$

The characteristic function of the interference associated to first order diffraction is given by

$$\phi_{D,1}(t) = \exp \left[ -2\lambda_S \int_0^L 1 - \exp \left[ -2\lambda_B \int_{r_0}^L 1 - \left[ 1 - jtP_B\kappa^{-1}(x+y+qxy)^{-\alpha_N^t} \right]^{-1} dx \right] dy \right]. \quad (30)$$

2) *User located at a crossroad:* Conditioned on  $r$ , the distance between the typical UE and its serving BS, the characteristic function of the useful received power is given by

$$\phi_{S,2}(t, \alpha|r) = \phi_{S,1}(t, \alpha|r). \quad (31)$$

Conditioned on  $r$ , the characteristic function of the LOS interference coming from the typical street and avenue is given by

$$\phi_{L,2}(t|r) = \phi_{L,1}^2(t|r). \quad (32)$$

Conditioned on  $r$ , the characteristic function of the NLOS interference coming from the typical street and avenue is given by

$$\phi_{N,2}(t|r) = \phi_{N,1}^2(t|r). \quad (33)$$

The characteristic function of the interference associated to first order diffraction is given by

$$\phi_{D,2}(t) = \phi_{D,1}^2(t|r). \quad (34)$$

### B. Coverage probability

The coverage probability for a typical street UE and crossroad UE can be computed as follows:

$$\begin{aligned} P_{c,i}(\theta) &= \frac{1}{2} + \frac{1}{\pi} \int_0^\infty \text{Im} \left[ \phi_{D,i}(-\theta t) \int_{r_0}^\infty p_L(r) \phi_{S,i}(t, \alpha_L^t|r) \phi_{L,i}(-\theta t|r) \phi_{N,i}(-\theta t|r) f_{r,i}(r) dr \right] t^{-1} dt \\ &+ \frac{1}{\pi} \int_0^\infty \text{Im} \left[ \phi_{D,i}(-\theta t) \int_{r_0}^\infty p_N(r) \phi_{S,i}(t, \alpha_N^t|r) \phi_{L,i}(-\theta t|r) \phi_{N,i}(-\theta t|r) f_{r,i}(r) dr \right] t^{-1} dt \quad (35) \end{aligned}$$

where  $i = 1$  for a street UE and  $i = 2$  for a crossroad UE.

Since the general typical user is located at a crossroad with probability  $\eta$  and in a street with probability  $1 - \eta$ , using the law of total probability, the general coverage probability is obtained as follows

$$P_c(\theta) = (1 - \eta)P_{c,1}(\theta) + \eta P_{c,2}(\theta). \quad (36)$$

### C. Exposure CDF

The exposure CDF for a typical street UE and crossroad UE can be computed as follows:

$$\begin{aligned} P_{e,i}(\theta) &= \frac{1}{2} + \frac{1}{\pi} \int_0^\infty \text{Im} \left[ e^{-jt\theta} \phi_{D,i}(t) \int_{r_0}^\infty p_L(r) \phi_{S,i}(t, \alpha_L^t|r) \phi_{L,i}(t|r) \phi_{N,i}(t|r) f_{r,i}(r) dr \right] t^{-1} dt \\ &+ \frac{1}{\pi} \int_0^\infty \text{Im} \left[ e^{-jt\theta} \phi_{D,i}(t) \int_{r_0}^\infty p_N(r) \phi_{S,i}(t, \alpha_N^t|r) \phi_{L,i}(t|r) \phi_{N,i}(t|r) f_{r,i}(r) dr \right] t^{-1} dt \quad (37) \end{aligned}$$

where  $i = 1$  for a street UE and  $i = 2$  for a crossroad UE.

As for the coverage probability, the general exposure CDF is obtained using the law of total probability as follows

$$P_e(\theta') = (1 - \eta)P_{e,1}(\theta') + \eta P_{e,2}(\theta'). \quad (38)$$

#### *D. Lower bound on the joint SIR-exposure distribution*

The joint SIR-exposure distribution lower bound for a typical street UE and crossroad UE can be computed as follows:

$$\bar{F}_i(\theta, \theta') = \max\left(0, P_{c,i}(\theta) - (1 - P_{e,i}(\theta'))\right) \quad (39)$$

where  $i = 1$  for a street UE and  $i = 2$  for a crossroad UE.

As for the coverage probability, the general joint SIR-exposure distribution lower bound is obtained using the law of total probability as follows

$$\bar{F}(\theta, \theta') = (1 - \eta)\bar{F}_1(\theta, \theta') + \eta\bar{F}_2(\theta, \theta'). \quad (40)$$

#### *E. Capacity CCDF*

The capacity CCDF for a typical street UE and crossroad UE can be computed as follows:

$$P_{cap,i}(\theta'') = P_{c,i}\left(2^{\frac{\theta''}{B}} - 1\right) \quad (41)$$

where  $i = 1$  for a street UE and  $i = 2$  for a crossroad UE.

As for the coverage probability, the general capacity CCDF is obtained using the law of total probability as follows

$$P_{cap}(\theta'') = (1 - \eta)P_{cap,1}(\theta'') + \eta P_{cap,2}(\theta''). \quad (42)$$

TABLE I: Network parameters

Variable	Symbol	Value	Explanation
Area's edge	$L$	4km	For accurate statistics
UE/BS/buildings heights	$h_U/h_B/h_{BU}$	1.5m/6m/20m	Realistic values
Streets and avenues densities	$\lambda_S$	5/km	Realistic values in Manhattan
BS densities	$\lambda_B$	5/km	/
BS power	$P_B$	1W	/
Frequency	$f$	3.6GHz	For small cells deployment
Typical street/avenue fading	$h_{ij}^{t,L}$ and $h_{ij}^{t,N}$	Rice $K(r) = 6$	/
Perpendicular streets/avenues fading	$h_{ij}^{p,N}$	Rayleigh	/
LOS pathloss coefficient	$\alpha_L^t$	1.7	/
NLOS pathloss coefficients	$\alpha_N^t/\alpha_L^p$	2.5/3.5	/
Crossroad probability	$\eta$	0.1	/
LOS probability in the typical street	$P_L(r)$	$e^{-0.004r}$	/

#### IV. NUMERICAL RESULTS

Numerical parameters used in the following results are summarized and explained in Table I. Unless stated otherwise in the different sections, those parameters remain unchanged.

##### A. Impact of the LOS probability $P_L(r)$

In this section, the impact of the LOS probability  $P_L(r)$  in the typical street is quantified. [20] gives us a completely general LOS probability  $(1 - P_\infty) \exp\left(-\left(\frac{r}{\alpha}\right)^N + P_\infty\right)$  where  $r$  is the distance and  $P_\infty$  is the probability to be in LOS at an infinite distance. As expected, this expression ensures automatic LOS when the distance is 0. In this work, we assume the LOS probability is 0 at an infinite distance and we simplify the expression as  $\exp(-\beta r)$ . Moreover, we make the parameter  $\beta$  vary in order to model how abrupt the LOS probability is. The higher  $\beta$  is, the quicker we lose LOS with the distance. Figure 5 and 6 respectively show the impact of  $P_L(r)$  on the coverage probability and the exposure CDF. In addition, analytical results are validated

using Monte Carlo simulations and compared to the case where LOS is assumed regardless of the distance.

Regarding the impact on the coverage probability, it strongly depends on how progressively the LOS is lost. If the LOS is more progressively lost as it is the case for  $\beta = 0.004$ , two opposite scenarios happen:

- 1) In some cases, the serving BS (the closest one) is not in LOS but some interferers might still be in LOS. This deteriorates the coverage probability and questions the relevance of the closest BS association policy with respect to the strongest BS association policy.
- 2) The serving BS stays in LOS and interferers have lower probability to be in LOS. This enhances the coverage probability.

Both scenarios explain why the coverage probability is lower for small values of the SIR threshold (due to scenario 1) and higher for high values of the SIR threshold (due to scenario 2).

If LOS is rapidly lost as it is the case for  $\beta = 0.04$ , interferers are almost automatically not in LOS and scenario 1 vanishes. This means that for any value of the SIR threshold, for an environment where the LOS quickly disappears with distance and regarding the fixed pathloss coefficients, we end up making a big underestimation of the coverage probability if this LOS probability is not implemented in the model. In addition, regardless of the LOS probability, this underestimation error is done for the interesting values of the SIR (above 5dB).

As the NLOS BSs have lower contributions to the total observed power, the impact on the exposure CDF is quite straightforward and easily explained. In fact, implementing the LOS probability limits the contributions of further BS hence a left-shifted CDF in case of abrupt LOS-NLOS transition. As a consequence, we end up making a big overestimation of the exposure if this LOS probability is not implemented in the model which might be misleading regarding the

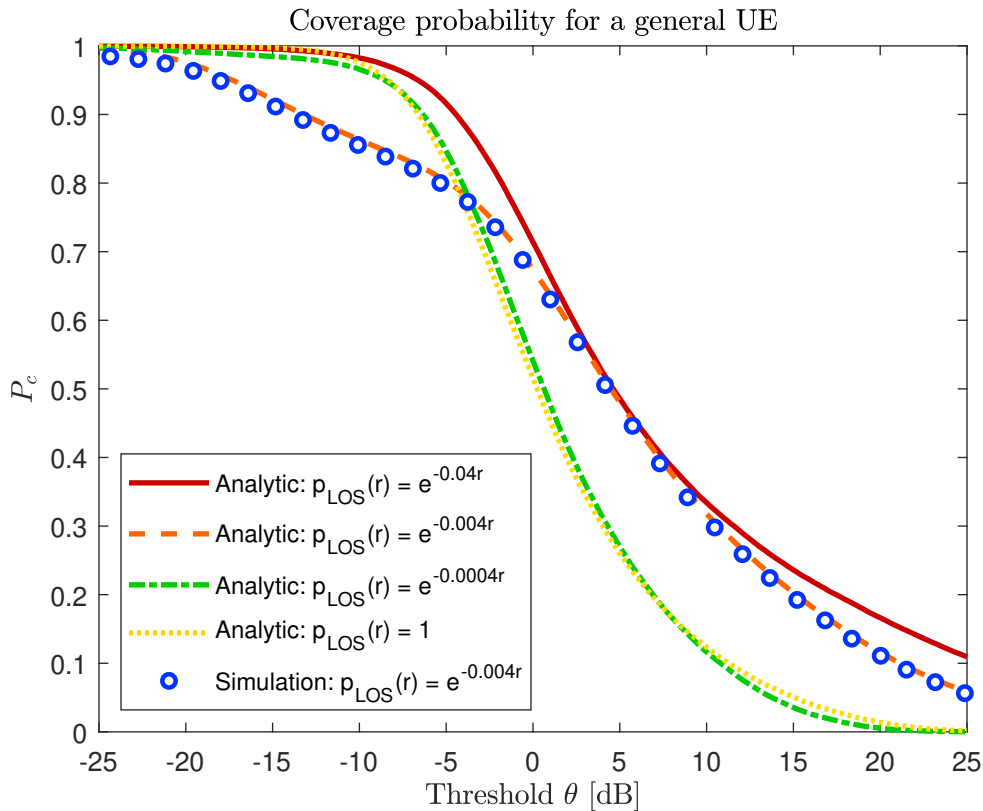


Fig. 5: Coverage probability for a general UE: varying  $\beta$

potential densification limit if legal exposure thresholds have to be respected

### B. Impact of the crossroad probability $\beta$

In this section, the impact of the crossroad probability  $\eta$  is quantified. This impact is here evaluated on the coverage probability as it is shown on Figure 7. It can be seen that, by increasing the crossroad probability  $\eta$ , we progressively switch from the street UE ( $\eta = 0$ ) to the crossroad UE ( $\eta = 1$ ). In the literature, only the street UE is generally considered and its respective coverage probability is thus assumed to be representative of the general performances. In reality, if the crossroad probability is not negligible, the street UE performances is here proved not to be representative as a different  $\eta$  modifies the coverage probability .

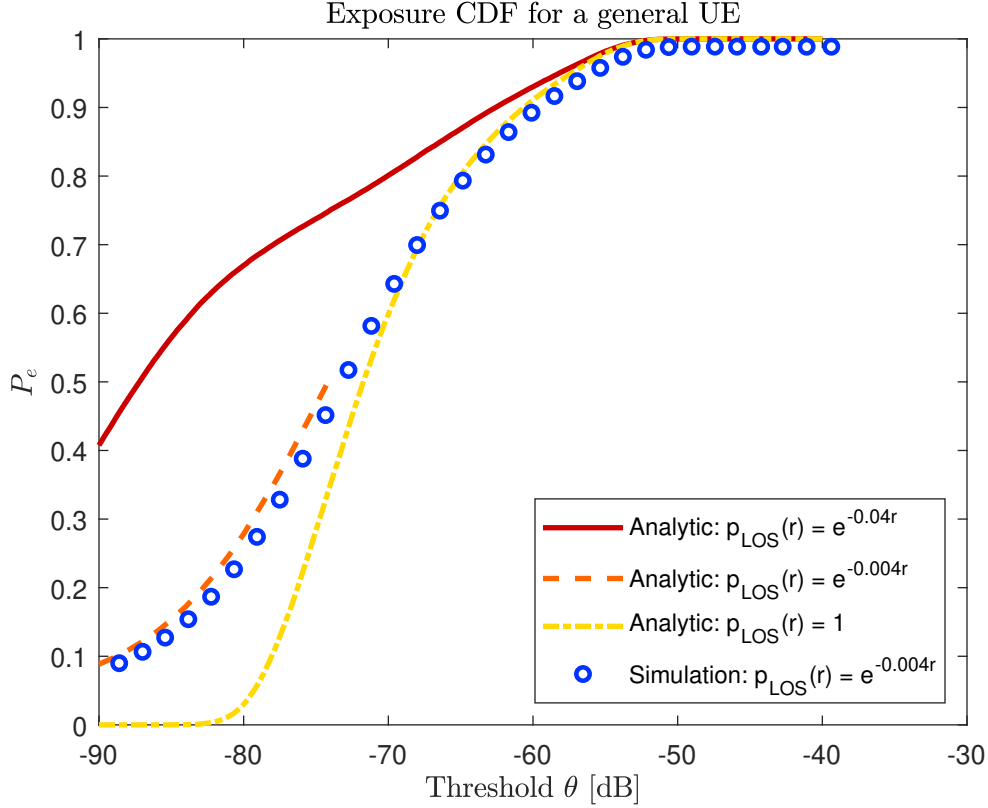


Fig. 6: Exposure CDF for a general UE: varying  $\eta$

As a crossroad UE experiences LOS contributions from both its typical street and avenue and receives diffracted contributions from both perpendicular streets and avenues, its respective exposure is on average doubled with respect to the street UE. If the crossroad probability is not negligible, the street UE performances is proved to underestimate the real exposure.

### C. Impact of the antenna height difference $dH$

In this section, the impact of the antennas heights difference  $dH$  is quantified. Figure 8 shows the coverage probability for  $dH=4,5\text{m}$  and  $dH=1\text{m}$  which corresponds to the usual SG models (that handle the singularity of the single slope model in  $r=0$ ). It is shown that for high values of the SIR which happen to be the values of interest, we slightly overestimate the coverage probability by neglecting this height difference. This comes from the fact that it mainly impacts

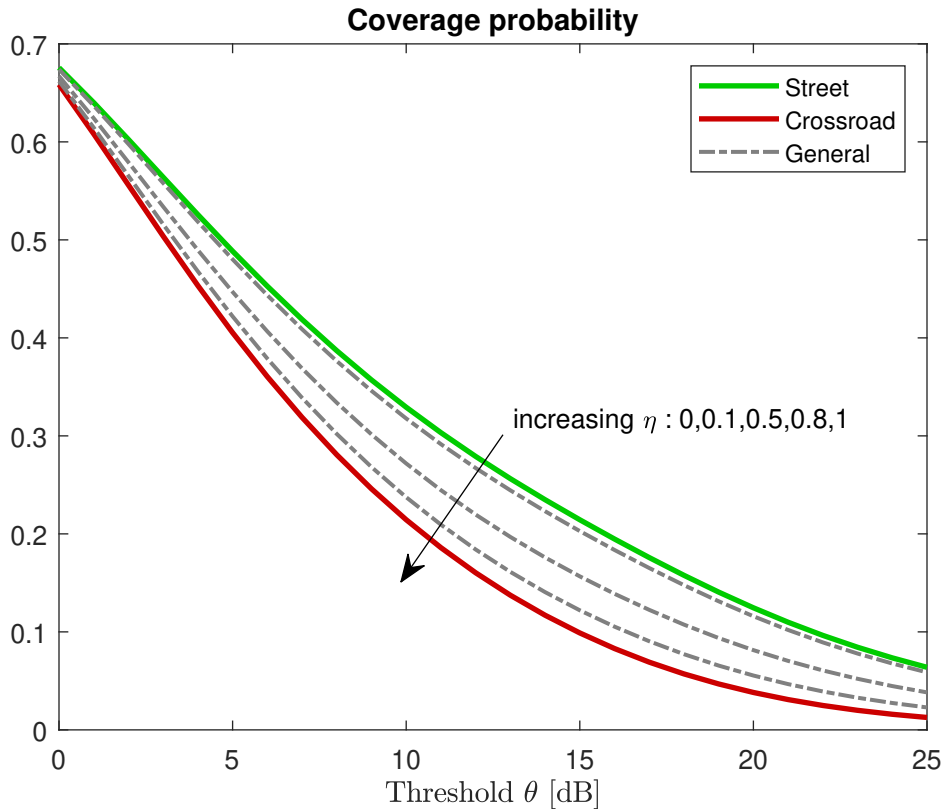


Fig. 7: Coverage probability for a general UE: varying  $\eta$

the contributions originating from close BSs as the antenna height difference is negligible for long distance links. As a consequence, the serving BS received power is generally overestimated while other contributions present lower errors. This results in a misleadingly high SIR therefore boosting the coverage probability.

#### D. Comparison to ray tracing

In this section, the similarities and differences between the SG model and the RT algorithm will be highlighted for different metrics of interest. In the framework of this analysis, we thus launch 3500 RT simulations with the same environments characteristics ( $\lambda_S$  and  $\lambda_B$ ) as if they were MC simulations and compute the received power  $P_{RT,[W]}^{i^*j}$  at the typical UE.

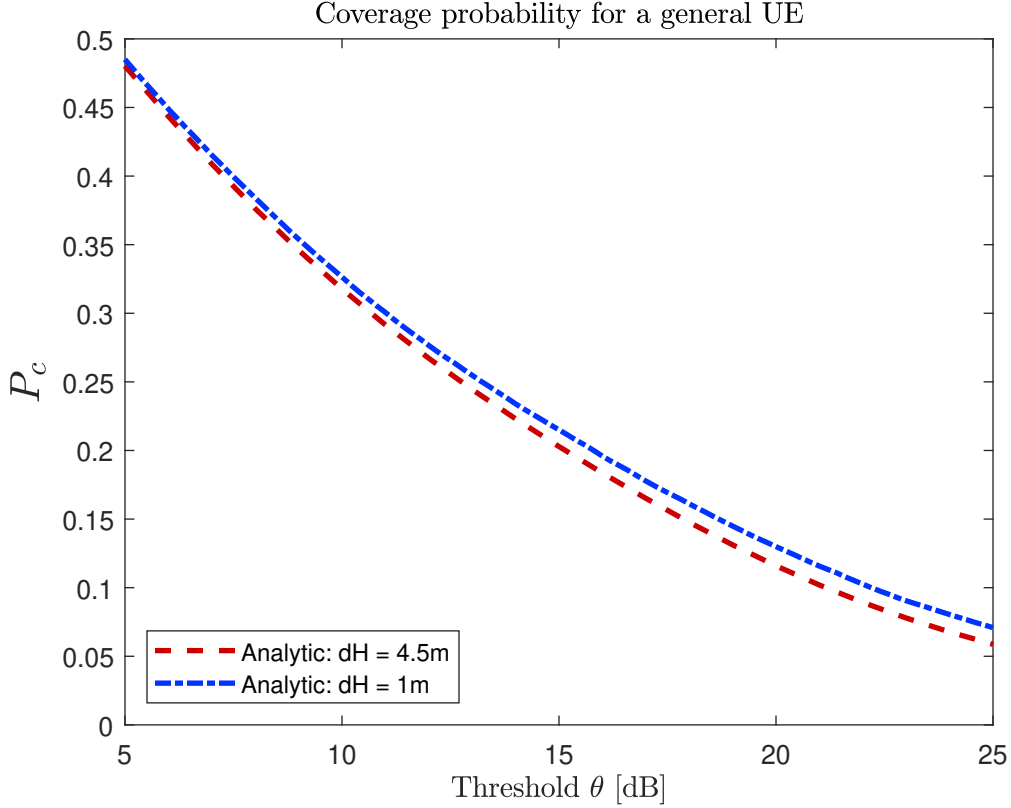


Fig. 8: Coverage probability for a general UE: varying dH

In order to create a LOS probability in the RT algorithm, we generate obstacles (cars and trucks) with a certain density in the typical street and avenue. We then compute the parameters  $\beta$  and  $N$  for  $p_L(r) = \exp(-\beta r^N)$  to fit the observed RT LOS probability by minimizing the mean square error (MSE). This expression is then used in our SG model. In addition, we compute the observed RT crossroad probability  $\eta$ .

In order to fix the pathloss coefficients in the typical street and avenue, we compare  $P_{RT,[W]}^{i*j} \frac{\kappa}{P_B}$  to the single slope model  $\frac{1}{r^\alpha}$ . We fix their values in order to minimize the MSE. Once those coefficients found, we fix the corresponding fadings by comparing  $P_{RT,[W]}^{i*j} \frac{\kappa}{P_B} r^\alpha$  to different fading distributions. A summary of the different parameters can be found in Table II

TABLE II: Network parameters

Variable	Symbol	Value	Explanation
Area's edge	$L$	4km	For accurate statistics
UE/BS/buildings heights	$h_U/h_B/h_{BU}$	1.5m/6m/20m	Realistic values
Streets and avenues densities	$\lambda_S$	5/km	Realistic values in Manhattan
BS densities	$\lambda_B$	5/km	/
BS power	$P_B$	1W	/
Frequency	$f$	3.6GHz	For small cells deployment
Typical street/avenue fading	$h_{ij}^{t,L}$ and $h_{ij}^{t,N}$	Rayleigh	Fitting (observation)
Perpendicular streets/avenues fading	$h_{ij}^{p,N}$	Rayleigh	/
LOS pathloss coefficient	$\alpha_L^t$	1.74	Fitting (MMSE)
NLOS pathloss coefficients	$\alpha_N^t/\alpha_L^p$	1.77/3.5	Fitting (MMSE)
Crossroad probability	$\eta$	0.02	/
LOS probability in the typical street	$P_L(r)$	$e^{-0.004r^{0.85}}$	Fitting (MMSE)
Ground and wall permittivity	$\epsilon_{ground}$ $\epsilon_{wall}$	15-1.4986i 5.3-0.4166i	Values fixed based on [16] for given frequency
Streets and avenues width	$w_S$	35m	Realistic value in Manhattan
Wall-BS Distance	$d_{B,BU}$	5m	Fixed Value

Figure 9 shows that, by properly tuning the parameters of our SG model, it is possible to obtain fairly accurate statistics for both the coverage probability and the exposure CDF. As shown on Figure 10, the observed differences comes from the fact that the CDF of the serving BS contribution is right-shifted while we correctly evaluate the interference. This makes us overestimate the coverage probability and the exposure.

## V. CONCLUSION

In this document, we considered a Manhattan-like environment and analyzed different metrics of interest for a typical central UE. This UE can either be at a crossroad, be in a street or be a completely general UE. Closed-form expressions or semi-closed form expressions of the

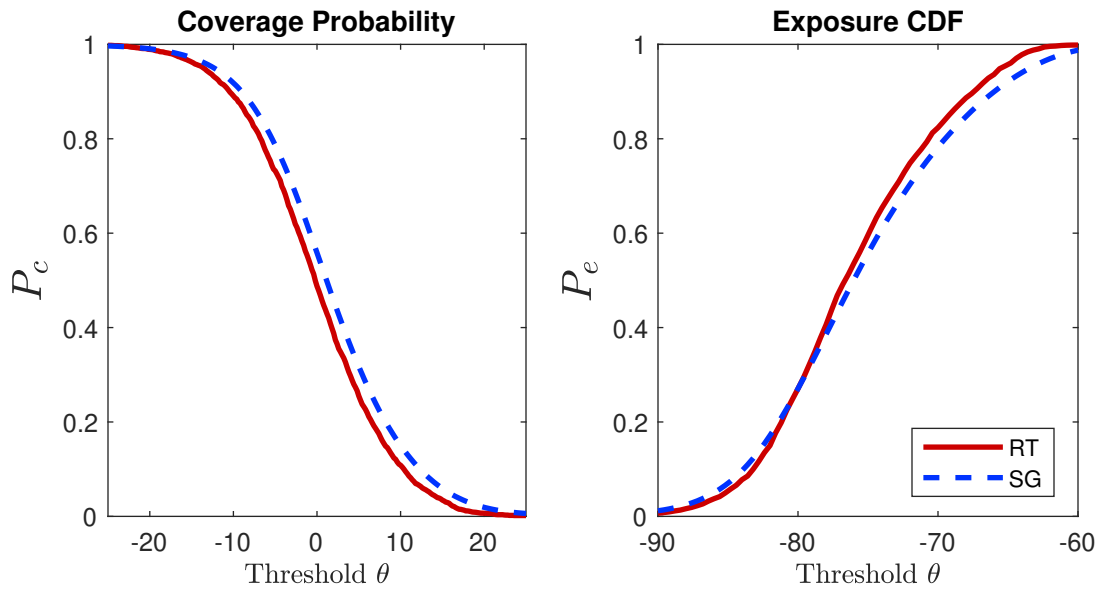


Fig. 9: Comparison of SG and RT approaches on the coverage probability and the exposure CDF

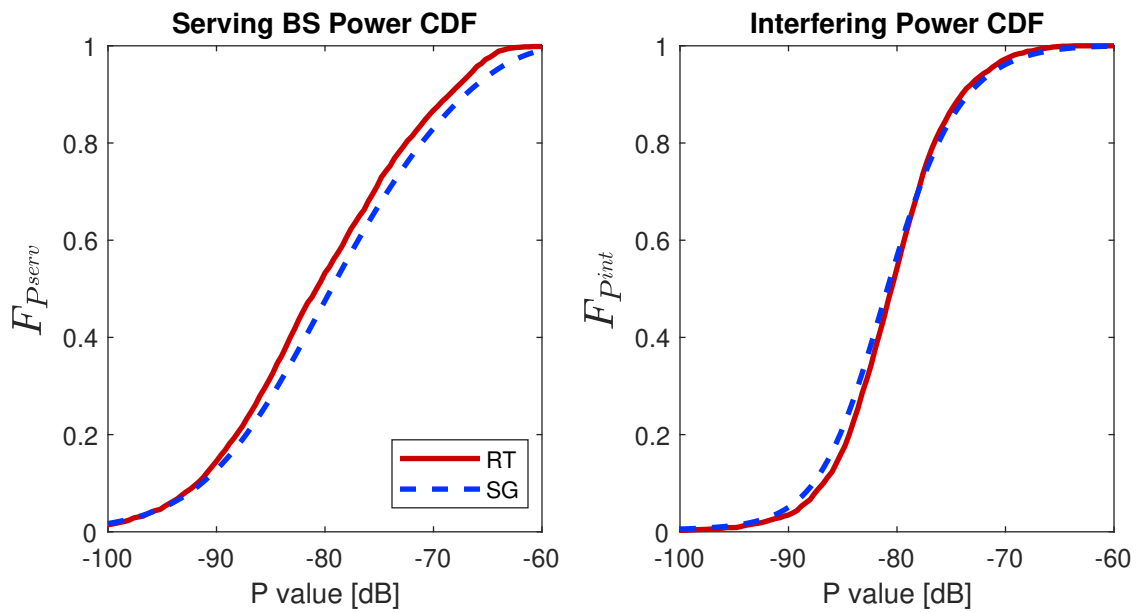


Fig. 10: Comparison of SG and RT approaches on the serving BS power CDF and the interfering BS power CDF

coverage probability, the CDF of the exposure, the CDF of the UE capacity and a lower bound on the joint SIR-Exposition probability have been derived.

It has been shown that:

- Not implementing the LOS probability in a model makes us underestimate the coverage probability and overestimate the exposure.
- Not taking into account the possibility that a UE can be at a crossroad implies a mistake on the coverage probability and an underestimation of the exposure if the crossroad probability is non negligible.
- Not taking the antenna heights into account wrongly boosts the coverage probability for interesting values of the SIR threshold.
- Our SG model gives fair statistics in terms of coverage probability and exposure if parameters are tuned adequately.

Further research directions could include the implementation of beamforming schemes inside our SG model, implementing other propagations mechanisms in the RT tool and comparison of those results with Winner type channel models.

#### ACKNOWLEDGMENT

Computational resources have been provided by the supercomputing facilities of the Université catholique de Louvain (CISM/UCL) and the Consortium des Équipements de Calcul Intensif en Fédération Wallonie Bruxelles (CÉCI) funded by the Fond de la Recherche Scientifique de Belgique (F.R.S.-FNRS) under convention 2.5020.11 and by the Walloon Region.

#### REFERENCES

- [1] M. K. Weldon, *The future X network: a Bell Labs perspective*. CRC press, 2016.

- [2] K. Ali, “Modeling, analysis, and design of 5g networks using stochastic geometry,” Ph.D. dissertation, 2018.
- [3] A. Osseiran, J. F. Monserrat, and P. Marsch, *5G mobile and wireless communications technology*. Cambridge University Press, 2016.
- [4] X. Ge, S. Tu, G. Mao, C.-X. Wang, and T. Han, “5g ultra-dense cellular networks,” *IEEE Wireless Communications*, vol. 23, no. 1, pp. 72–79, 2016.
- [5] Y. Hmamouche, “Applications of stochastic geometry in the modeling and analysis of wireless networks,” Ph.D. dissertation, Ecole nationale supérieure Mines-Télécom Atlantique, 2020.
- [6] F. Baccelli and X. Zhang, “A correlated shadowing model for urban wireless networks,” in *2015 IEEE Conference on Computer Communications (INFOCOM)*. IEEE, 2015, pp. 801–809.
- [7] Y. Wang, K. Venugopal, A. F. Molisch, and R. W. Heath, “Mmwave vehicle-to-infrastructure communication: Analysis of urban microcellular networks,” *IEEE Transactions on Vehicular Technology*, vol. 67, no. 8, pp. 7086–7100, 2018.
- [8] V. V. Chetlur and H. S. Dhillon, “Coverage analysis of a vehicular network modeled as cox process driven by poisson line process,” *IEEE Transactions on Wireless Communications*, vol. 17, no. 7, pp. 4401–4416, 2018.
- [9] —, “On the load distribution of vehicular users modeled by a poisson line cox process,” *IEEE Wireless Communications Letters*, vol. 9, no. 12, pp. 2121–2125, 2020.
- [10] X. Lu, M. Salehi, M. Haenggi, E. Hossain, and H. Jiang, “Stochastic geometry analysis of spatial-temporal performance in wireless networks: A tutorial,” *IEEE Communications Surveys & Tutorials*, 2021.
- [11] W. Lu and M. Di Renzo, “Stochastic geometry modeling of cellular networks: Analysis, simulation and experimental validation,” in *Proceedings of the 18th ACM International Conference on Modeling, Analysis and Simulation of Wireless and Mobile Systems*, 2015,

- pp. 179–188.
- [12] S. S. Ram, G. Singh, and G. Ghatak, “Optimization of radar parameters for maximum detection probability under generalized discrete clutter conditions using stochastic geometry,” *arXiv preprint arXiv:2101.12429*, 2021.
- [13] J.-E. Berg, “A recursive method for street microcell path loss calculations,” in *Proceedings of 6th International Symposium on Personal, Indoor and Mobile Radio Communications*, vol. 1. IEEE, 1995, pp. 140–143.
- [14] C. Wiame, L. Vandendorpe, and C. Oestges, “Stochastic geometry based coverage estimation using realistic urban shadowing models,” in *2018 IEEE 87th Vehicular Technology Conference (VTC Spring)*. IEEE, 2018, pp. 1–5.
- [15] J. Gil-Pelaez, “Note on the inversion theorem,” *Biometrika*, vol. 38, no. 3-4, pp. 481–482, 1951.
- [16] C. Oestges, “Propagation modelling of low earth-orbit satellite personal communication systems,” PhD dissertation, Universite Catholique de Louvain, 2000.
- [17] D. Tami, C. G. Rego, D. Guevara, A. Navarro, F. J. Moreira, J. Giménez, and H. G. Triana, “Analysis of heuristic uniform theory of diffraction coefficients for electromagnetic scattering prediction,” *International Journal of Antennas and Propagation*, vol. 2018, 2018.
- [18] L. Raschkowski, P. Kyösti, K. Kusume, and T. Jämsä, “Metis channel model,” in *ICT-317669-METIS/D1.4*, 2015.
- [19] S. Wang, W. Guo, and M. D. McDonnell, “Distance distributions for real cellular networks,” in *Computer Communications Workshops (INFOCOM WKSHPS), 2014 IEEE Conference on*. IEEE, 2014, pp. 181–182.
- [20] J. Järveläinen, S. L. Nguyen, K. Haneda, R. Naderpour, and U. T. Virk, “Evaluation of millimeter-wave line-of-sight probability with point cloud data,” *IEEE Wireless Communications Letters*, vol. 5, no. 3, pp. 228–231, 2016.